Exploring Power Quality in Hybrid Microgrids: Investigating an SVM Inverter-Fed Induction Motor Drive and Modulation Index Diversity

Dr. S. Vasantharaj
Assistant Professor, Dept. of Electrical and Electrical Engg
Kings College of Engineering
Thanjavur
vasantharaj118@gmail.com

Dr. S. Naveen Prakash
Assistant Professor, Dept. of Electrical and Electrical Engg
Kings College of Engineering
Thanjavur
naveeneee.kce@gmail.com

V. Veeraselvan
UG Students, Dept. of Electrical and Electrical Engg
Kings College of Engineering
Thanjavur
vselvan904@gmail.com

P. Milton Infant Rai
UG Students, Dept. of Electrical and Electrical Engg
Kings College of Engineering
Thanjavur
milton979192@gmail.com

***Abstract*— The effects of varying the modulation indices on the current and voltage harmonics of an induction motor (IM) powered by a three-phase space vector pulse width modulation (SVM) inverter are presented in this research. The effects have been examined using simulation and an experimental setup. IM can be governed by an SVM inverter drive or a phase angle control drive for applications which require varying speeds. The analysis of THD content in this study uses the modulation index (MI), whose modification affects the harmonic content and the usage of voltage-oriented control (VOC) with SVM in three-phase pulse width modulation (PWM) inverters with fixed switching frequencies. The control technique relies on two cascaded feedback loops, one controlling the grid current and the other regulating the dc-link voltage, with the purpose of maintaining the required level of dc-bus voltage. The control strategy was developed to transform between stationary (α – β) and synchronously rotating (d - q) coordinate systems.**

Keywords*— i*nduction motor drive; dc–link voltage balancing; space vector modulation; switching loss; total harmonic distortion

I. INTRODUCTION

Electric motors are being used in a growing number of driving components around the world, accounting for 40% to 50% of all electricity demand [1]. 70% of the electricity needed to run industrial loads is provided by three phase IM [2]. Due to its appealing qualities, such as their low cost, straightforward design, excellent reliability, and ease of maintenance, electric motor sales have climbed to 85%. Despite the fact that direct current (DC) motors are frequently seen in applications involving variable speed operations because of how simple it is to control torque and field flux with armature and field current, these motors possess drawback of having a commutator and brushes, that could cause corrosion and necessitate regular maintenance [3]. Due to its high output power, toughness, robustness, efficiency, affordability, capacity to tolerate hazardous or severe working situations, and ruggedness, IM's do not experience DC motor difficulties [4]. The abrupt variation in load, which uses a significant amount of electricity and raises the cost of energy, has an impact on the functioning of three phase IM. To regulate speed and preserve high efficiency, a variable speed drive (VSD) may be employed. Moreover, the controller and switching technique employed in VSD have a significant impact on achieving high efficiency and reliability for IM's [5]. Pulse Width Modulation (PWM) techniques are often used to control the switches of voltage source inverters (VSIs), as well as the frequency and output voltage of IMs. One of the better approaches for VSI is the SVM switching approach, which has reduced switching losses and the capacity to reduce the harmonic output signals generated by inverters.

Recent studies have proposed several control techniques for PWM rectifiers in order to enhance the input power factor and transform the input current into a sinusoidal waveform. There are numerous PWM modulation techniques in use, including sinusoidal PWM and the space vector method. Technically, the SVM methodology has been shown to be the optimal modulation method overall. Compared to the conventional PWM approach, the harmonic distortion of current is decreased with the SVM. The duty cycle of the VSI switches was determined using the SVM using the space vector concept. The only thing that has been digitally implemented are PWM modulators. The ability for straightforward digital implementation and a large linear modulation range for line-to-line voltages are the distinguishing features of SVM. Despite the SVPWM technique's benefits over PWM, new ways are continually being developed. The main objective was to find efficient methods to provide output voltages with low harmonic rates and less switch-level loss.

The voltage-oriented control (VOC) algorithm, which is well known among indirect power control algorithms that use current controllers and is equivalent to the field-oriented control (FOC) of the IM, is allowed to generate high dynamic and static performance by using internal current control loops and an outer voltage control loop. The basis of VOC is the orientation of the rotating synchronous reference frame with respect to the grid line voltage vector. The suggested VOC approach exhibits highly dynamic behaviour, suitable output voltage, and a low input current THD.

II. OVERVIEW OF INDUCTION MOTOR DRIVE

The squirrel-cage three-phase IM is a type of asynchronous AC motor that operates on electromagnetic induction principles. The IM's primary purpose is to convert electrical

energy into mechanical energy. A small air gap separates the stator and the rotor, which are the two components that make up the IM. The three-phase squirrel-cage IM [6 – 8] is the most often used due to its insulated winding in both stator and rotor, that are formed of cast and solid bars with high conductivity, as shown in figure 1.

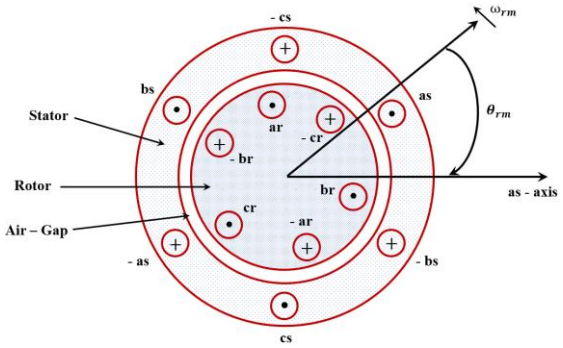

Fig 1: Three-phase IM cross-sectional model.

In order for the rotor to rotate at synchronous speed (ω_{sm} in rad/sec), where $\omega_{sm} = 2\pi f$ (rad/sec), where f = synchronous frequency, three phase voltages must first be applied to the stator winding. The stator currents produce a revolving magnetic field in the magnetic circuit, which is formed by the air gap between the stator and rotor cores. The number of poles affects the mechanical synchronous speed (ω_{sm} in rad/sec) or (N_{sm} in rpm) (P). This is how the synchronous speed is determined.

$$\omega_{sm} = \frac{2\omega_s}{P} \quad (1)$$

$$N_{sm} = \frac{120f}{P} \quad (2)$$

To depict the physical systems, the computer models the mathematical model of the three-phase IM and its driving system [4]. The control parameters of the models are highlighted in this three-phase IM modelling. For the three-phase IM, the magnetic connection between the stator and rotor voltage equations can be expressed as follows.

$$V_{as} = i_{as}r_s + \frac{d\lambda_{as}}{dt};\ V_{bs} = i_{bs}r_s + \frac{d\lambda_{bs}}{dt};\ V_{cs} = i_{cs}r_s + \frac{d\lambda_{cs}}{dt} \quad (3)$$

$$V_{ar} = i_{ar}r_r + \frac{d\lambda_{ar}}{dt};\ V_{br} = i_{br}r_r + \frac{d\lambda_{br}}{dt};\ V_{cr} = i_{cr}r_r + \frac{d\lambda_{cr}}{dt} \quad (4)$$

where V_{as}, V_{bs}, V_{cs} = 3-φ stator voltages; V_{ar}, V_{br}, V_{cr} = 3-φ rotor voltages; i_{as}, i_{bs}, i_{cs} = 3-φ stator currents; i_{ar}, i_{br}, i_{cr} = 3-φ rotor currents; r_s = stator resistance; r_r = rotor resistance; λ_{as}, λ_{bs}, λ_{cs} = flux linkages of the stator; and λ_{ar}, λ_{br}, λ_{cr} = flux linkages of the rotor.

According to the winding currents and inductances, the flux linkages indicate the matrix formed between the rotor and stator windings, as depicted in the subsequent matrix.

$$\begin{bmatrix}\lambda_s^{abc}\\ \lambda_r^{abc}\end{bmatrix} = \begin{bmatrix}L_{ss}^{abc} & L_{sr}^{abc}\\ L_{rs}^{abc} & L_{rr}^{abc}\end{bmatrix}\begin{bmatrix}i_s^{abc}\\ i_r^{abc}\end{bmatrix} \quad (5)$$

Where $\lambda_s^{abc}=[\lambda_{as}\ \ \lambda_{bs}\ \ \lambda_{cs}]^T$, $i_s^{abc}=[i_{as}\ \ i_{bs}\ \ i_{cs}]^T$, $\lambda_r^{abc}=[\lambda_{ar}\ \ \lambda_{br}\ \ \lambda_{cr}]^T$, $i_r^{abc}=[i_{ar}\ \ i_{br}\ \ i_{cr}]^T$ and superscript T = transpose of the array. The L_{ss}^{abc} = stator-to-stator winding inductance. L_{rr}^{abc} = rotor-to-rotor winding inductance, and L_{sr}^{abc} = stator-to-rotor mutual inductance depends on the rotor angle θ_r.

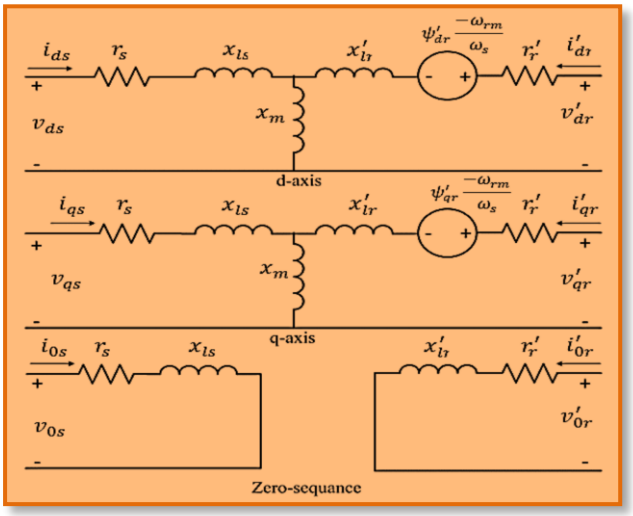

Fig 2. Equivalent circuits of the three-phase IM's dq0 stationary reference frames.

III. VOLTAGE-ORIENTED CONTROL

The VOC technique for AC-DC converters is derived from FOC for IMs. FOC provides a quick, dynamic reaction due to the utilization of current control loops. The theoretical elements of the VOC approach used for grid-connected rectifiers have received extensive coverage. The PWM technique is used by the control system to ensure that the characteristics of the VOC control scheme are modified. It is possible to reduce the impact of interference (disturbances). By using the hysteresis pulse-width modulation approach, system solidity is achieved. Power switching is stressed as a result of the fluctuating switching frequency, necessitating the use of an input filter at high-value parameters. In order to alleviate harmonics issues, the proposed method utilizes the VOC principle to regulate charging while maintaining low harmonic distortions to the grid. Figure 3 depicts VOC for AC-DC line-side converters. VOC operates most frequently in the two-phase 0 and dq0 domains, where the Clarke and Park transformation matrices are employed.

$$\begin{bmatrix}V_{s\alpha}\\ V_{s\beta}\\ V_0\end{bmatrix} = \sqrt{\frac{2}{3}}\begin{bmatrix}1 & \frac{-1}{2} & \frac{-1}{2}\\ 0 & \frac{\sqrt{3}}{2} & -\frac{\sqrt{3}}{2}\\ \frac{1}{\sqrt{2}} & \frac{1}{\sqrt{2}} & \frac{1}{\sqrt{2}}\end{bmatrix}\begin{bmatrix}V_{sa}\\ V_{sb}\\ V_{sc}\end{bmatrix} \quad (6)$$

$$\begin{bmatrix}V_d\\ V_q\end{bmatrix} = \begin{bmatrix}sin(\theta) & cos(\theta)\\ -cos(\theta) & sin(\theta)\end{bmatrix}\begin{bmatrix}V_{s\alpha}\\ V_{s\beta}\end{bmatrix} \quad (7)$$

Note that V_{sa}, V_{sb} and V_{sc} = 3-φ source voltages in abc domain, $V_{s\alpha}$, $V_{s\beta}$ and V_0 = source voltages of αβ0 domain. V_d, V_q and V_0 source voltages of dq0 domain, and θ = operating phase of the power system. As shown in Figure 2, an equivalent transformation procedure is used to transform the 3-φ source current i_{sabc}.

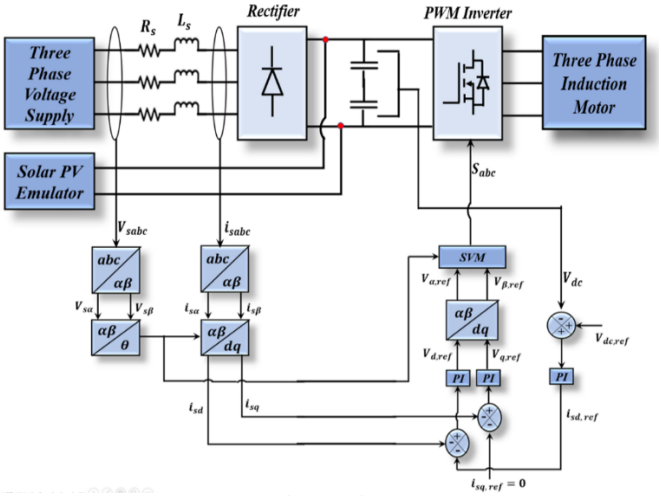

Fig 3. Overall control structure of VOC of a PWM inverter. [30].

IV. SVM SWITCHING TECHNIQUES

The SVM approach, generally acknowledged as the optimum way for variable speed drive applications, creates PWM control signals in the 3-φ inverter. Compared to other PWM systems, this method has an enhanced method for achieving a high output voltage, minimizing the harmonic output, and lowering switching losses. As a result, the SVM technique is confirmed as the best approach for reducing harmonic distortion [9].

$$\begin{bmatrix} V_{ab} \\ V_{bc} \\ V_{ca} \end{bmatrix} = V_{dc} \begin{bmatrix} 1 & -1 & 0 \\ 0 & 1 & -1 \\ -1 & 0 & 1 \end{bmatrix} \begin{bmatrix} S_1 \\ S_3 \\ S_5 \end{bmatrix} \quad (8)$$

$$\begin{bmatrix} V_{ab} \\ V_{bc} \\ V_{ca} \end{bmatrix} = \frac{V_{dc}}{3} \begin{bmatrix} 2 & -1 & -1 \\ -1 & 2 & -1 \\ -1 & -1 & 2 \end{bmatrix} \begin{bmatrix} S_1 \\ S_3 \\ S_5 \end{bmatrix} \quad (9)$$

Eight switch variables can be created using the inverter's six IGBTs. Six of these switch variables—V_1, V_2,..., V_6, and the last two—are zero vectors that were chosen for the three upper IGBT switches. The lower IGBT switches on and off patterns are the opposite of those of the higher switches. Using (8) and (9), the voltage space vectors (V_0, V_1.., V_7, etc).

The output waveform of the inverter is split into six hexagonal sectors according to the SVM's working principle. The sector angle is 60^0 apart, and every sector is between two voltage space vectors (figure 5). The SVM approach receives a 3-φ voltage (V_a, V_b, and V_c) with a 120^0 angle among the 2-φ and transforms it into 2-φ (V_α and V_β) with a 90^0 using Clark's transformation (figure 5 (a)).

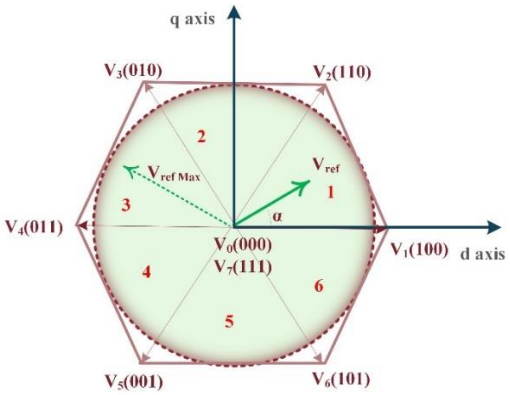

Fig 4. Space vector diagram.

To make the study of three-phase voltage more straightforward, 2-φ voltages (V_α and V_β) are used as a scientific transformation. The voltages are used to calculate the hexagon's voltage vectors angle (α) and reference voltage vector's magnitude (V_{ref}). The V_{ref} is assumed as the magnitude of the V_α and V_β voltages, while α is the frequency of the V_α and V_β. V_{ref} and α are situated among the two neighboring non-zero vectors and the zero vectors. The following formulas can be used to calculate them [10].

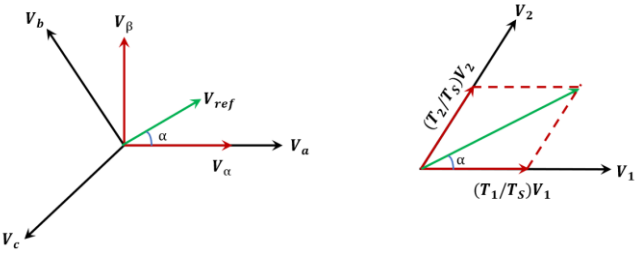

Fig 5. (a) Space vector diagram (b) Space of sector-1 between V_1 and V_2.

$$\begin{bmatrix} V_\alpha \\ V_\beta \end{bmatrix} = \frac{2}{3} \begin{bmatrix} 1 & \frac{-1}{2} & \frac{-1}{2} \\ 0 & \frac{\sqrt{3}}{2} & -\frac{\sqrt{3}}{2} \end{bmatrix} \begin{bmatrix} V_a \\ V_b \\ V_c \end{bmatrix} \quad (10)$$

$$|V_{ref}| = \sqrt{V_\alpha^2 + V_\beta^2} \quad (11)$$

$$\alpha = tan^{-1} \frac{V_\beta}{V_\alpha} \quad (12)$$

Sector 1 contains the vectors that can be used to synthesize V_{ref}, which is located here.

The relevant space vectors and time intervals (T_1; T_2; and T_0) in sector 1 are depicted in figure 5 (b). The duration of Vref is calculated by multiplying the reference voltage by the sampling time period, which is equivalent to the sum of the voltages times the time interval of the space vectors in the specified sector.

$$\int_0^{T_S} \bar{V}_{ref} dt = \int_0^{T_1} \bar{V}_1 dt + \int_{T_1}^{T_1+T_2} \bar{V}_2 dt + \int_{T_1+T_2}^{T_S} \bar{V}_0 dt$$
$$T_s = T_1 + T_2 + T_0 \quad (13)$$

Where *Ts* = switching time which is calculated by $Ts = \frac{1}{f_s}$, and *fs* = switching frequency.

Eq. (13) illustrates how $\overline{V_0}$ provides zero voltage to the output load. As a result, the equation is:

$$T_s \bar{V}_{ref} = T_1 \bar{V}_1 + T_2 \bar{V}_2 \quad (14)$$

When the values of $\overline{V_1}$ and $\overline{V_2}$ from Table 1 are substituted into the αβ frame and the voltage vectors are evaluated, the results are as follows:

$$T_s |V_{ref}| \begin{bmatrix} cos(\alpha) \\ sin(\alpha) \end{bmatrix} = T_1 \frac{2}{3} V_{dc} \begin{bmatrix} 1 \\ 0 \end{bmatrix} + T_2 \frac{2}{3} V_{dc} \begin{bmatrix} cos\frac{\pi}{3} \\ sin\frac{\pi}{3} \end{bmatrix} \quad (15)$$

$$T_1 = T_s \frac{3}{2} \frac{|V_{ref}|}{V_{dc}} \frac{sin(\frac{\pi}{3} - \alpha)}{sin(\frac{\pi}{3})} \quad (16)$$

$$T_2 = T_s \frac{3}{2} \frac{|V_{ref}|}{V_{dc}} \frac{sin(\alpha)}{sin(\frac{\pi}{3})} \quad (17)$$

The relation amongst the magnitude of the reference voltage and the DC voltage value represented by the following equation is known as the MI for the SVM.

$$MI = \frac{|V_{ref}|}{\frac{2}{\pi}V_{dc}} \quad (18)$$

Eq. (17) can be substituted into (15) and (16) to get the time duration in the other sectors (n), and 60 degrees with α can be used for each sector to get the result:

$$T_1 = \frac{\sqrt{3}T_s|V_{ref}|}{V_{dc}} sin(\frac{n}{3}\pi - \alpha) \quad (19)$$

$$T_2 = \frac{\sqrt{3}T_s|V_{ref}|}{V_{dc}} sin(\alpha - \frac{n-1}{3}\pi) \quad (20)$$

$$T_0 = T_s - (T_1 + T_2) \quad (21)$$

Alternating zero vector sequence, asymmetric sequence, maximum current not switched sequence and right aligned sequence are the four different types of switching patterns. The following two requirements must be fulfilled by all switching patterns in order to reduce device switching frequency. Merely two switches in the same inverter leg are used to switch from one switching state to another. To minimize the switching frequency, one of the switches must be turned off if the other is activated. The least amount of switching is necessary to move Vref from one sector to the next in order to minimize switching losses. The optimum strategy, according to research, is the symmetric sequence method since it minimizes switching losses. The generation of the SVM signal, inverter output voltages, and a comparison of the duty ratio waveform's three signals with the triangle waveform are shown in figure 6. The assumption behind this comparison is that S is ON if $V_{DutyRatio} > V_{triangle}$; else, S is OFF.

Every switch in a bipolar switching scheme operates in opposition to the facing switch, as seen in the example where the triangle waveform and the $V_{TaDutyRatio}$ are compared to produce the PWM signal for the IGBT1 and the opposing IGBT4 in leg 1, which is the identical as leg 2 and leg 3.

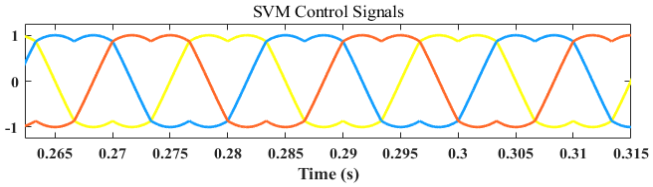

Figure 6. SVM waves for a three-phase inverter.

V. RESULTS AND DISCUSSION

In simulation studies, a number of experiments were carried out to confirm the effectiveness of the suggested VOC system. The DG capacities of the MG test system taken into consideration in this work are as follows. The SPV system has a 400-V output voltage rating with a 1-kW capacity. The load that is being taken into consideration is a three-phase, 1-hp squirrel cage IM connected at 415 V and 50 Hz.

The voltage control has been set up so that each of the following requirements is satisfied.

1) Decentralized control has been achieved normally.

2) Under diverse system situations, the whole MG closed-loop model is stable.

3) All of the associated DGs follow the reference signal that the SVM algorithm provides.

Each controller must successfully uphold the aforementioned three requirements and offer a reliable control inside its application domain. The software platform MATLAB/Simulink has been used to implement the entire system. The SVM method is used to evaluate if a PV system which is connected to a grid can improve power quality at the consumer terminals. Figure 7 depicts the creation of the SVM signal. The voltage waveforms and the current waveform share some phase and are both totally sinusoidal which is shown in figure 7. Figure 8 illustrates how the speed of 1425 rpm performed while the load torque remained constant at 3.0 N-m which is shown in figure 9. In accordance with carrier frequencies of 1 kHz and a MI of 0.9 (figure 10), Figure 11 displays an FFT analysis of the current and voltage in the system under consideration. The THD_i and THD_v values are respectively 1.10% and 1.22%. Figure 12 depicted the voltage on the dc-link capacitor.

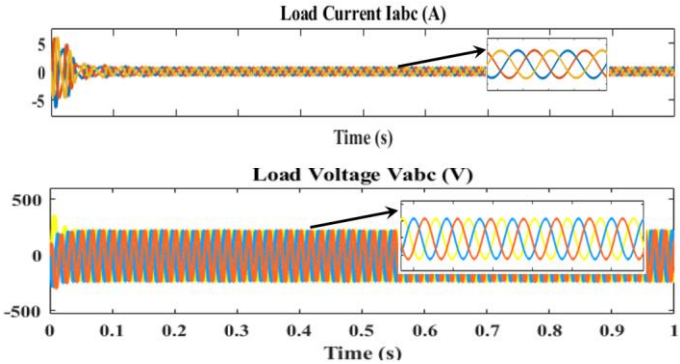

Fig 7: Current and Voltage waveform of IM with VOC based SVM Controller.

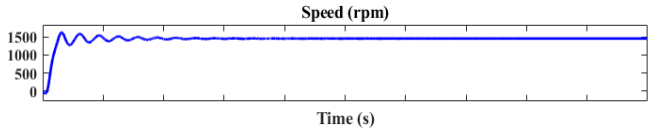

Fig 8: Speed of Induction Motor when MI = 0.9.

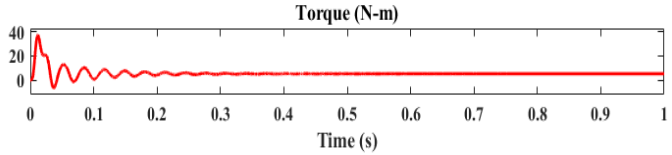

Fig 9: Torque of Induction Motor.

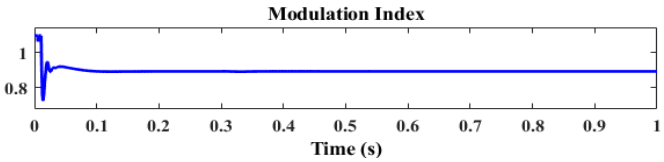

Fig 10: Modulation Index.

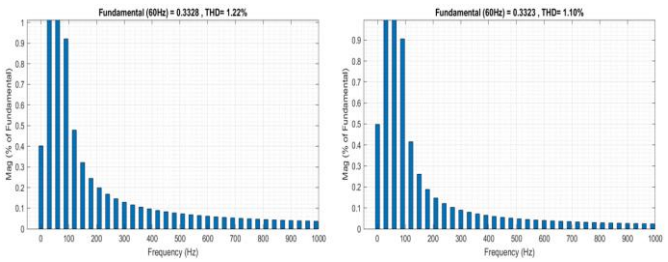

Fig 11: FFT analysis of voltage and current of Induction Motor.

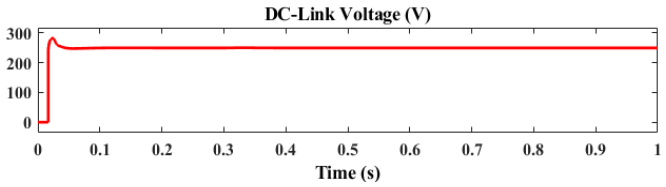

Fig 12: DC – Link voltage.

The optimum output signal is created by increasing the MI with the use of the SVM technique, as can be seen in figure 13. It is also evident that increasing the MI results in a decrease in current and voltage harmonics. Figure 14 shows the change in speed with MI.

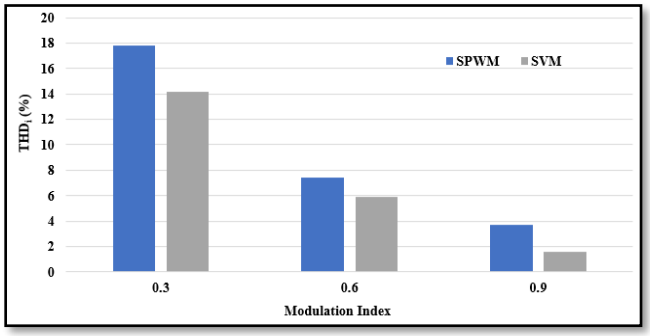

Fig 13. Comparison of Current THD with SPWM and SVM techniques.

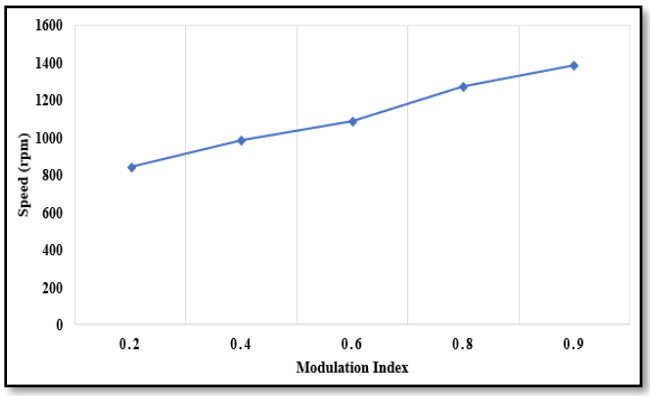

Fig 14. Change in speed Vs MI.

VI. CONCLUSION

In this study, the SVM employing PI controller was evaluated after taking the negative impacts of harmonics in a power system network into account. An SVM control technique has been devised to reduce current harmonics and increase power quality. Pollution-free electricity generation via PV systems has been prioritized along with improving power quality. This research paper focuses on the harmonic analysis of a three-phase PWM inverter that supplies IM using a variety of modulation indices. However, because losses are greater at very high switching frequencies, the work is constrained. By creating suitable controls and switching methods, the motor's speed can be controlled. In MATLAB, a three-phase PWM inverter that supplies IM is modelled. Results indicate that the IEEE Standard 519 standard limit of 5% for harmonic content in voltage and current is exceeded. Additionally, it is found that THD declines as MI rises. Future research can use a variety of PWM techniques to reduce harmonics while maintaining MI constant. Each scenario's harmonic analysis was properly adjusted to the IEEE-519 standard's limitations.

REFERENCES

[1] S.-M. Lu, “A review of high-efficiency motors: Specification, policy, and technology," *Renew. Sustain. Energy Rev.*, vol. 59, pp. 1_12, Jun. 2016.
[2] A. T. de Almeida, J. Fong, H. Falkner, and P. Bertoldi, “Policy options to promote energy efficient electric motors and drives in the EU," *Renew. Sustain. Energy Rev.*, vol. 74, pp. 1275_1286, Jul. 2017.
[3] R. Saidur, S. Mekhilef, M. B. Ali, A. Safari, and H. A. Mohammed, ``Applications of variable speed drive (VSD) in electrical motors energy savings," *Renew. Sustain. Energy Rev.*, vol. 16, no. 1, pp. 543_550, Jan. 2012.
[4] C. M. F. S. Reza, M. D. Islam, and S. Mekhilef, ``A review of reliable and energy efficient direct torque-controlled induction motor drives," *Renew. Sustain. Energy Rev.*, vol. 37, pp. 919_932, Sep. 2014.
[5] Al-Ogaili, A. S., Aris, I. B., Verayiah, R., Ramasamy, A., Marsadek, M., Rahmat, N. A., & Al-Masri, A. N. (2019). A three-level universal electric vehicle charger based on voltage-oriented control and pulse-width modulation. *Energies*, *12*(12), 2375.
[6] Hakami, S. S., Mohd Alsofyani, I., & Lee, K. B. (2020). Low-speed performance improvement of direct torque control for induction motor drives fed by three-level NPC inverter. Electronics, 9(1), 77.
[7] B. M.Wilamowski and J. D. Irwin, Power Electronics and Motor Drives. Boca Raton, FL, USA: CRC Press, 2011.
[8] A. Djoudi, S. Bacha, H. Iman-Eini, and T. Rekioua, ``Sliding mode control of DFIG powers in the case of unknown _ux and rotor currents with reduced switching frequency," Int. J. Electr. Power Energy Syst., vol. 96, pp. 347_356, Mar. 2018.
[9] H. Guzman, F. Barrero, and M. J. Duran, ``IGBT-gating failure effect on a fault-tolerant predictive current-controlled five-phase induction motor drive," IEEE Trans. Ind. Electron., vol. 62, no. 1, pp. 15_20, Jan. 2015.
[10] M. A. Hannan et al., ``A quantum lightning search algorithm-based fuzzy speed controller for induction motor drive," IEEE Access, vol. 6, pp. 1214_1223, 2018.